Trace element accumulation in Mn-Fe-oxide nodules of a planosolic horizon.

Sophie Cornu, Valérie Deschatrettes, Sébastien Salvador-Blanes, Blandine Clozel, Michel Hardy, Stéphane Branchut, Lydie Le Forestier

Trace element accumulation in Mn—Fe—oxide nodules of a planosolic horizon

Sophie Cornu[a], Valérie Deschatrettes[a], Sébastien Salvador-Blanes[a], Blandine Clozel[b], Michel Hardy[a], Stéphane Branchut[c] and Lydie Le Forestier[c]

[a]INRA Orléans, Unité de sciences du sol, Avenue de la pomme de pin, BP 20619, 45166 Olivet Cedex, France
[b]BRGM, 3 av. C. Guillemin, BP 6009, Orléans Cedex 2, France
[c]ISTO (UMR 6113 CNRS-Université d'Orléans), Polytech'Orléans, 8 rue Léonard de Vinci, 45072 Orléans Cedex 2, France

Keywords: Trace metal; Iron; Manganese; Nodule; Speciation; Planosol

The aim of this work was to determine the importance of nodule formation on the dynamics of major and trace elements (TEs) along a Planosol toposequence developed in metamorphic parent material at La Châtre (Massif Central, France). The different horizons were sampled within three pits and analysed for major and trace element contents. The nodule-rich horizon was studied more closely. A simplified sequential extraction scheme, X-ray diffraction (XRD) and microscopic approaches were used in order to determine the individual phases containing TE in nodules.

Along the slope, the nodule-rich horizon varies in thickness, is composed of different oxide fractions and has different scavenging efficiencies according to the TE considered. Iron was found to accumulate in the middle of the slope, while Mn accumulated at the base. The scavenging effect is only evident for Ni in profile 1. For Fe and Cu, it is maximal in profile 2 where the nodule-rich horizon is the thickest. For Pb and Mn, maximal scavenging effect is recorded for both profiles 2 and 3, in the lowest part of the slope. Cr is not accumulated at all. This was related to the water dynamic and the hydromorphic conditions prevailing along the slope.

Results obtained by sequential extractions and associated X-ray diffraction on the different nodule size fractions and those obtained by electron microprobe allow inference of the TE distribution in nodules. Nodules were mainly composed of three to four types of cements surrounding grains of quartz, feldspars, micas and accessory minerals: iron-rich cements, Si- and Al-rich cements, Mn-rich cements and Ti-rich cements in places.

The iron-rich cements consist of poorly crystalline goethite and possibly some ferrihydrite. Ferrihydrite is associated with Cr as demonstrated by extractions. Goethite contained Mn and most of the TE extracted except for Ni and Pb.

Fine-grained Si- and Al-rich cements were also observed. They contain variable amounts of Ti and Mn.

Mn-rich cements were not present in all the nodules and were mainly linked to the dark zones of the nodules. The nature of these Mn oxides could not be determined. They were found to contain Co, Ni, Cu and probably Pb.

1. Introduction

Trace elements (TEs) are well known for their high affinity for iron and manganese oxides (Alloway, 1990 and McBride, 1994). Fe and Mn oxides are abundant in soils. The Fe oxides include hematite, goethite, lepidocrocite, maghemite, magnetite, ferrihydrite and amorphous hydroxide (Oades, 1963). Mn oxide mineralogical phases classically encountered in soils are birnesite and vernadite (McKenzie, 1989). In all cases, Mn and Fe oxides are active TE sinks (Chao and Theobald, 1976, McKenzie, 1989, Singh and Gilkes, 1992 and Trolard et al., 1995). For example, Mn oxides are known to contain Co, Ni and Zn (Childs and Leslie, 1977), and goethite and hematite may contain Mn, Ni, Cr, Co, Cu and Zn (Singh and Gilkes, 1992). This is a result of either their ability to sorb TEs at their surface or of coprecipitation during formation (Jenne, 1968 and McKenzie, 1989). These mechanisms have been extensively studied in laboratory experiments (Loganathan et al., 1977, Schwertmann et al., 1989 and Dario and Ledin, 1997). Mn oxides are less abundant in soils than Fe oxides and have been proven to have a higher adsorption capacity in soil. This is because their point of zero charge (PZC) is low, varying from 2 to 5 (McKenzie, 1989), compared to that of Fe oxides ranging from 6.8 to 8 (Childs and Leslie, 1977). Thus, Mn oxides have a negative surface charge at pH values usually encountered in soil. This favours adsorption of TE cations at their surface (McKenzie, 1989).

Fe and Mn oxides result from the weathering of primary minerals. They precipitate as coatings on other minerals and in nodules of different shapes. Coatings result in the development of large surface areas favouring adsorption processes. Nodules of Mn and Fe oxides have been studied in different soil types (Childs and Leslie, 1977, Dawson et al., 1985, Latrille et al., 2001, Palumbo et al., 2001 and Liu et al., 2002). They generally comprise both Mn and Fe oxides, both elements having a different spatial distribution within nodules (Dawson et al., 1985, Palumbo et al., 2001 and Liu et al., 2002). Si, Al, K, Ca and Ti are also encountered in large quantities in nodules (Latrille et al., 2001, Palumbo et al., 2001 and Liu et al., 2002). Co, Ni and Zn were frequently associated with the Mn-rich parts of nodules (Childs and Leslie, 1977, Dawson et al., 1985, Latrille et al., 2001 and Liu et al., 2002), while Cr (Liu et al., 2002) and Pb (Latrille et al., 2001 and Palumbo et al., 2001) were associated with Fe-rich parts. McKenzie (1975), Childs and Leslie (1977), Dawson et al. (1985), Latrille et al. (2001), Palumbo et al. (2001) and Liu et al. (2002) showed that Cu and Mn partitioning between Fe and Mn oxides in nodules was variable.

Oxides are sensitive to variations in pH and Eh. They dissolve under reducing or acidic conditions (Jenne, 1968). Mn oxides are dissolved at higher Eh and/or pH values than Fe oxides and are often precipitated as thermodynamically nonstable phases (Jenne, 1968). Oxides release TEs on dissolution (Cambier and Charlatchaka, 1999). They are thus both source and sink of TEs in the environment, and they control their concentrations in most soils and waters (Jenne, 1968). It is therefore crucial to understand their dynamics at the profile and landscape scale and their TE scavenging ability in order to predict the fate of TE in the environment. However, to our knowledge, only a few studies have attempted to demonstrate the impact of oxides on TE scavenging at the landscape scale (Childs and Leslie, 1977).

The aim of this work was to determine the importance of nodule formation to the fate of major and trace elements in Planosols along a toposequence. Planosols are characterised by the vertical succession of clay-poor horizons overlying a clay-rich horizon that drastically limits the vertical flow of water (Baize, 1989). Such a vertical differentiation induces lateral water transfer at the top of the clay-rich horizon. The overlying horizon is therefore generally leached and clay-poor. According to the water regime throughout the year, oxide nodules may develop at the base of this last horizon, forming a hard crust in places. This horizon accumulates or releases TE depending on the oxide formation/dissolution dynamic.

We studied element distribution in Planosols developed in metamorphic parent material at La Châtre, Massif Central, France. These soils are naturally rich in TE due to the regional geology and are subject to seasonal water saturation during winter and spring (Salvador-Blanes, 2002). Nodules of different sizes were analysed for their TE contents.

2. Material and methods

2.1. Soils

The study site, located on the Aigurande plateau in the Massif Central, is underlain by amphibolite and gneiss. On the crest and shoulder, soils have developed in amphibolite, while on the backslope, the soils were developed in gneiss. On the footslope, Planosols developed on gneiss (Salvador-Blanes, 2002).

The upper horizons of the Planosols are allochthonous and derived from colluvial materials of amphibolitic and gneissic origin, while the deeper B horizon (below 50 cm depth) and the alterite are developed in gneiss. Colluvial materials differentiate into three horizons: a sandy-loam to clay-loam organic-rich A horizon (25- to 30-cm thick) and two E horizons.

Three pits were dug along a toposequence (Fig. 1), differing mainly by their colluvial horizons, especially by the depth, thickness and pedological

characteristics of the E horizons. According to their location within the toposequence, three E horizons, noted E_1, E_2 and E_3, were defined. E_1 contains no concretions, while E_2 is characterised by its richness in concretions and E_3 in both concretions and gravel. They may also be differentiated by their colour and water content. In pit 1, E_3 is 10-cm thick and appears at a depth of about 30 cm, while in pits 2 and 3, E_2 and E_3 appear, respectively, about 30 and 20 cm depth, and E_2 and E_3 are respectively 35- to 45-cm thick and 10- to 20-cm thick. In addition, E_3 was indurated in places in pit 2 (Fig. 1). The E horizons are waterlogged during winter and spring, the intensity of which increase along the slope.

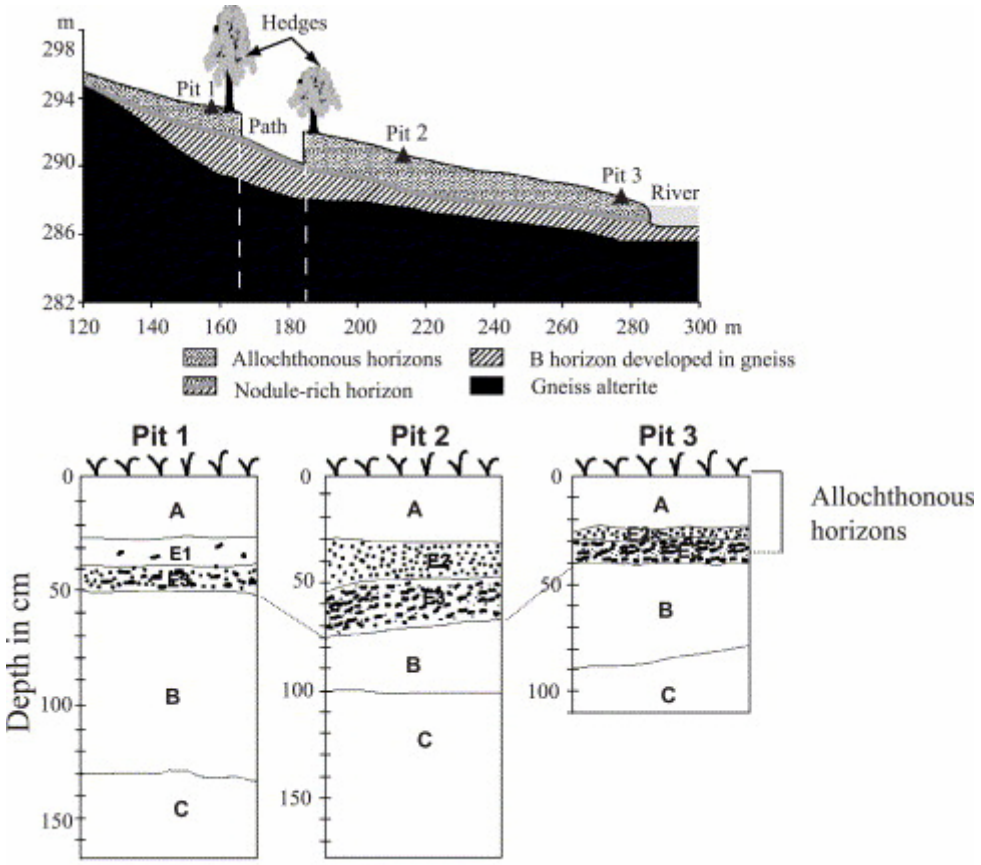

Fig. 1. Schematic diagram of the studied toposequence.

All horizons were sampled and air-dried. Nongravely horizons were analysed by ICP-OES, after triacidic digestion (HF, $HClO_4$ and HCl) for major and trace element contents. Si was analysed after alkaline fusion. Apparent densities were measured for stock calculation within the allochthonous horizons.

Nodule-rich horizons were fractionated by sieving into particle-size classes of <1, 1–2, 2–5, 5–20 and >20 mm. The different fractions were analysed for major and trace element contents as described above.

2.2. Fractionation and characterisation of the nodules

Nodules were sorted manually from the previously obtained particle size fractions for those classes larger than 1 mm and for the deepest nodule-rich horizon of pits 2 and 3 only. They were washed in milliQ water and separated into 1–2, 2–5 and 5–20 mm fractions. These fractions were analysed for major and trace element contents by ICP-OES after HF-triacidic dissolution. The poorly crystalline fraction was extracted after Hall et al. (1996) by 0.25 M hydroxylamine, HCl+0.25 M HCl at a solid/liquid ratio of 1:20 for 2 h at 60 °C, and subsequently, the crystalline fraction was extracted with 1 M hydroxylamine, HCl+25% acetic acid at a solid/liquid ratio of 1:30 for 3 h at 90 °C. Both extraction steps were performed three times. After each extraction step, a milli-Q water rinse was performed at a solid/liquid ratio of 1:20 for 1 h. The rinse solutions were added to the corresponding extracted solution. All reagents used were either Merck suprapure or Prolabo Normatom ultrapure grade. All extracts were analysed for Si, Al, Fe and Mn using ICP-OES. The limits of determination for these analyses were 20 µg l^{-1} for Mn and 0.1 mg l^{-1} for the remaining elements. Mg, K and Ca were determined using flame AAS, with 0.1, 0.1 and 0.5 mg l^{-1}, the respective limits of determination. ICP-MS was used to analyse extracts for Cu, Ni, Co, Cr, Zn and Pb. The limits of determination for these elements were 1, 1, 1, 2, 2 and 0.2 µg l^{-1}, respectively. Extraction results were expressed in mg/kg^{-1} for trace elements and for Mn and in percent (%) for major elements.

Solid residues were chemically analysed after the last extraction step. X-ray diffraction (XRD) analyses were performed on nodules before and after extractions. We used a X Philips PW 1710 diffractometer equipped with a Co cathode. Diffractograms were obtained for θ ranging from 36° to 48°, with steps of 0.02° measured over 50 s. The diffractograms obtained before and after extraction were subtracted in order to determine the suite of minerals that were dissolved through extractions (Schulze, 1981).

2.3. Microscopic analysis of the nodules

The indurated parts of the E_3 horizon were sampled in pit 2, air-dried and impregnated with polyester resin. Micropolished thin sections (45×60 mm) were made. In order to examine the interior structure of the nodules, a sample of 1- to 2-mm nodules from pit 2 were set in resin, cut to show a cross section and micropolished.

The thin sections were observed with a polarizing light microscope and scanning electron microscopy (SEM) using the backscattered electron mode. Both the optical and electron microscopes enabled characterisation of the nodule structure.

Spatial distribution of major chemical elements (Si–Al–Fe–Mg–K) within nodules was determined using a CAMECA SX 50 electron microprobe equipped with

wavelength-dispersive spectrometers (WDS). We used an acceleration voltage of 15 kV, a probe current of 4 nA and a count time equal to 13 s. The beam was 1 µm in diameter that led to an elemental analysis volume of about 3 to 5 μm^3. Both spot analysis and mapping were carried out. Some minor and trace elements were also analysed on 51 points within the cement zone of six 1- to 2-mm nodules. The electron microprobe detection limits were too high to allow a continuous mapping of TE in the nodules. The surfaces mapped were either 4×4 mm (map A, Fig. 2) or 2×2 mm (map B to E, Fig. 2).

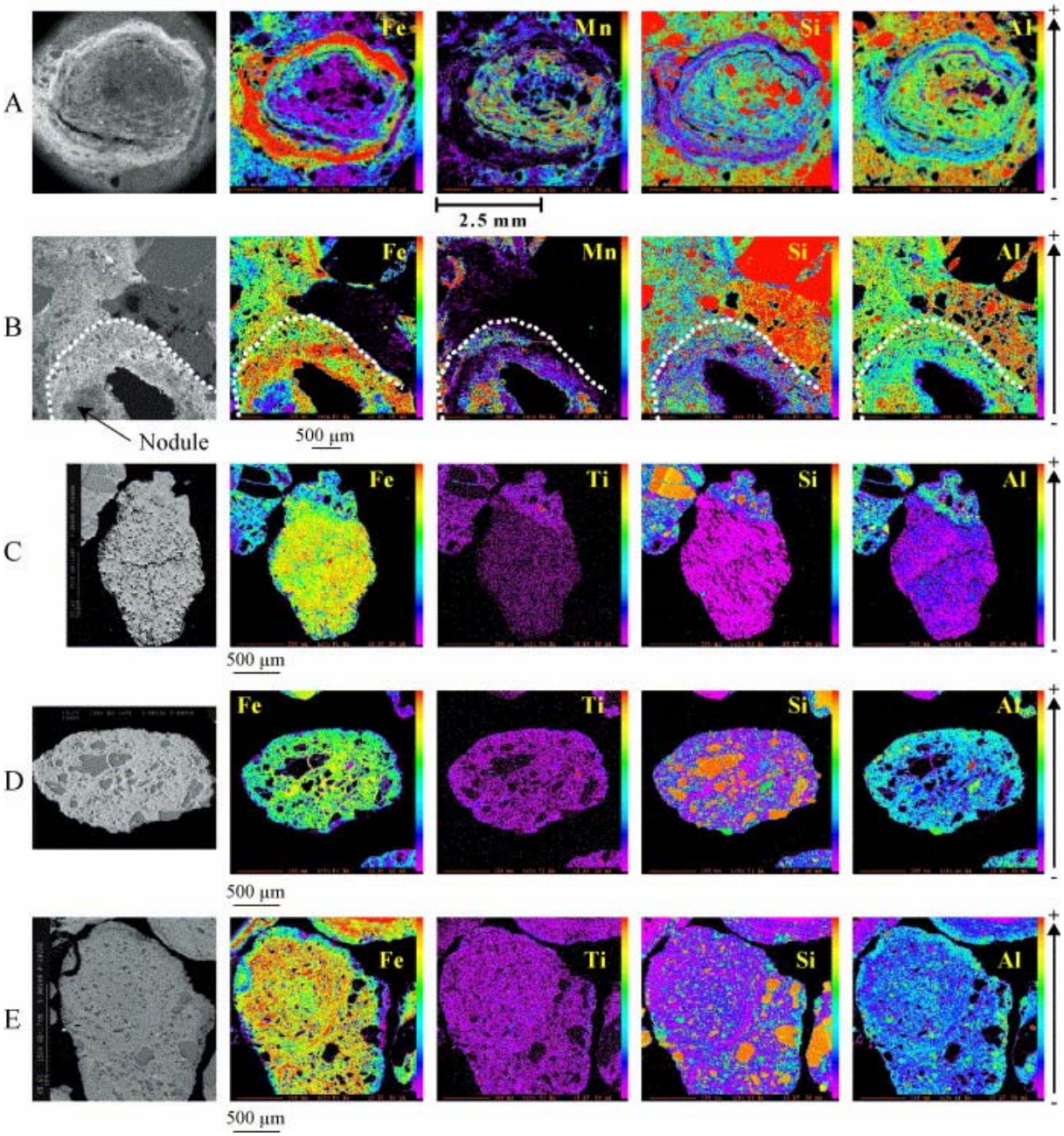

Fig. 2. TE spatial distribution in nodules (electron microprobe mapping). Five nodules are represented (A–E).

3. Results

3.1. Element distribution at the profile scale

Fig. 3 gives the chemical profiles of pits 1 to 3. The main variations in chemical contents along the slope were recorded for the nodule-rich horizons, where both the depths and chemical contents vary. These horizons are richer in Mn and Co (Fig. 3) than the upper allochthonous horizon. Enrichment factors were calculated and reported in Table 1 in order to compare the chemical composition of the nodule-rich horizons with that of the overlying allochthonous horizons, which were considered to have had the same original composition as the nodule-rich horizons. As well as high enrichment factors in Co and Mn, slight enrichments in Fe, Ni and in places, Cu, were also observed (Table 1). Nodule-rich horizons were depleted in all the other measured elements as shown by enrichment factors of less than 1 (Table 1). This was due to the mineral composition of these horizons comprising mainly quartz, with feldspars and micas to a lesser extent. Nodules were also abundant.

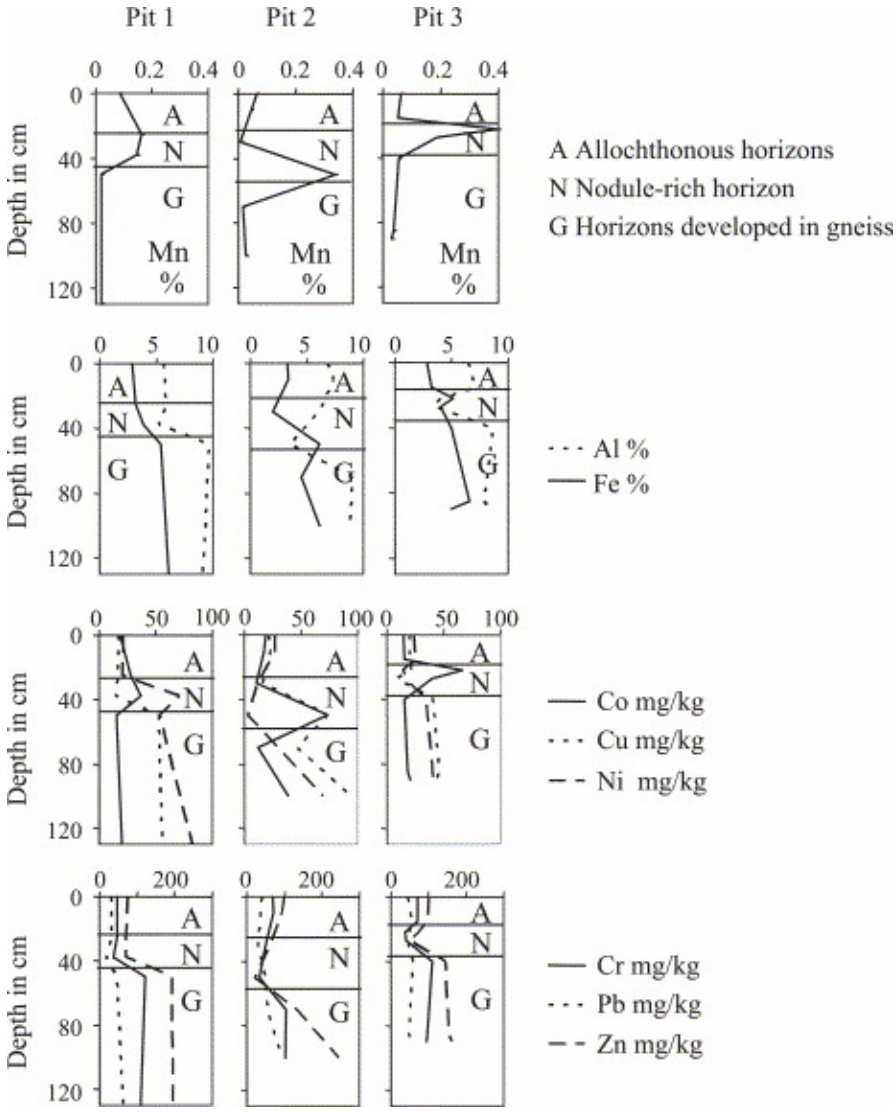

Fig. 3. Chemical profile of the three pits.

Along the slope, the Fe enrichment is highest in the deepest nodule-rich horizons of profile 2. It is associated with a strong Cu enrichment, which is absent from the other pits. Enrichment in Fe is also important in profile 3. Maximum enrichment of Mn and Co occurs in profile 3 and enrichment of Ni is observed for profile 1 only (Table 1). In addition, for profiles 2 and 3, the nodule-rich horizon is subdivided into two horizons (E_2 and E_3). In profile 2, the E_2 horizon is depleted in all the elements, while in profile 3, this horizon contains the richest concentration of Fe, Mn and Co (Table 1).

Stocks were calculated within the allochthonous horizons. They are reported in Table 2. For comparative purposes, stocks were divided by the thickness of the allochthonous horizons. Regardless of the position in the toposequence, stocks by centimeter were of the same order of magnitude for most elements, excluding K, Cu and Ni.

Table 1. : Enrichment factors in the nodule-rich horizons compared to the other allochthonous horizons for pits 1 to 3 (P1, P2, P3)

Pit	Horizon	Si	Al	Fe	Ca	Mg	Mn	K	Cr	Co	Pb	Cu	Ni	Zn
1	E_3	1.0	0.90	1.3	0.50	0.63	1.2	1.1	0.79	1.6	0.56	0.90	3.5	0.97
2	E_2	1.2	0.85	0.60	0.73	0.63	0.11	1.1	0.72	0.58	0.77	0.73	0.44	0.60
	E_3	0.82	0.50	1.3	0.36	0.27	6.0	0.65	0.49	4.1	1.3	3.3	0.12	0.22
3	E_2	1.3	0.60	1.7	0.43	0.40	6.9	0.66	0.55	4.4	0.98	1.1	0.57	0.75
	E_3	1.0	0.51	1.3	0.28	0.33	3.2	0.65	0.57	2.6	0.83	0.43	0.65	0.49

Table 2. : Element stocks in within the allochthonous horizons

Pit	Horizon	Depth, cm	Si	Al	Fe	Ca	Mg	K	Mn	Cr	Co	Pb	Cu	Ni	Zn
			g m^3						mg m^3						
1	A	0–25	1080	183	95	37	18	39	2822	156	59	100	54	68	243
	E_1	25–38	665	113	63	22	11	25	3202	94	56	61	31	39	137
	E_3	38–50	653	99	74	11	7	26	2794	73	72	33	28	136	136
	Total		2399	395	232	69	36	90	8818	323	187	194	113	243	516
	Stock/cm		48	8	5	1	1	2	176	6	4	4	2	5	10
2	A	0–30	1081	259	120	35	25	54	1871	252	63	132	81	96	341
	E_2	30–50	526	90	30	10	6	25	94	75	16	43	24	17	87
	E_3	50–70	924	134	231	13	7	37	12,926	130	281	185	278	13	79
	Total		2531	483	381	58	38	116	14,891	458	359	360	383	125	507
	Stock/cm		36	7	5	1	1	2	213	7	5	5	5	2	7
3	A	0–22	481	122	55	17	11	27	1073	128	27	90	36	44	179
	E_2	22–27	237	29	36	3	2	7	2797	27	47	34	15	10	51
	E_3	27–40	568	76	89	6	4	21	4177	89	89	91	19	36	106
	Total		1286	226	180	26	17	55	8047	244	163	215	70	90	337
	Stock/cm		32	6	4	1	0	1	201	6	4	5	2	2	8

3.2. Characterisation of the nodules: bulk approaches

The E_3 horizons from profiles 2 and 3 contain about one-third of particles >2 cm (mainly quartz) and two-fifths of nodules ranging from 1 mm to 2 cm (Table 3). The particle-size distribution of these nodules is about the same for profiles 2 and 3 (profile 1 was not studied in detail). In terms of mass, the largest nodules (5 to 20 mm) represent about two-thirds of the nodules, while the smallest sorted (1 to 2 mm) represent only a few percent (Table 3).

Elements enriched in nodules compared to the <1 mm fractions of profiles 2 and 3 (Table 4) are Fe, Mn and Co and to a lesser extent, Ni, Zn and Pb. Nodules are depleted in Si, Al, Mg, Ca and K. Enrichments vary according to the nodule size and to the position along the slope. In profile 2, enrichment factors increase with the nodule size for Mn, Co, Ni and Zn. Conversely, they decrease for Fe and Pb. In profile 3, the largest enrichment factors are recorded for the 2- to 5-mm nodules for most elements with the exception of Co, while the lowest ones are observed for the coarsest nodules. Co enrichment factors follow the same trend as seen in profile 2. Lastly, enrichment factors in profile 3 are lower for all of the measured elements than those in profile 2. Cu is the only element enriched in profile 3 nodules but not in those of profile 2.
Table 5 summarizes the correlation coefficients between TE and Mn and Fe in extracts 1 and 2 solutions; Co, Ni and Cu in extract 1 are correlated with Mn, while Fe is correlated with Cr. Zn and Pb are not correlated with either Mn or Fe. In extract 2, there is a strong relationship between Fe and Mn, Co, Cu and Zn, but less with Cr. No correlation was found with Ni and Pb.

Table 3. : Proportion and chemical composition of the different size fractions and nodule fractions of the E_3 horizons of pits 1 and 2

Pit		Particle size, mm	Weight, %	Si	Ca	Mg	K	Fe	Al	Mn	Cu	Zn	Cr	Ni	Co	Pb
				%						mg kg^{-1}						
		<1	32	34	0.44	0.36	1.9	1.9	6.5	322	54	64	58	14	12	33
2	Nodule-free material	1–2	3	42	0.18	0.03	0.39	0.64	1.4	38	2.8	9.5	6.7	2	1.2	9.6
		2–5	5	41	0.21	0.04	0.22	2.0	1.7	184	4.2	13	8.8	2.5	3.3	18
		5–20	6	45	0.02	0.02	0.07	0.37	0.26	127	73	8.2	7.5	3.3	1.0	6.3
	Nodules	1–2	1	25	0.39	0.17	0.9	18	4.3	3595	35	116	91	22	113	138
		2–5	9	26	0.33	0.20	1.0	18	4.1	4826	29	11	54	32	131	118
		5–20	21	22	0.74	0.20	1.1	17	4.1	13,410	23	128	43	42	271	116
		<1	24	32	0.45	0.50	2.2	2.5	7.7	505	17	95	72	22	11	45
3	Nodule-free material	1–2	4	44	0.15	0.03	0.37	0.42	1.4	32	2.2	10	5.8	2.0	0.7	11
		2–5	8	44	0.34	0.05	0.27	0.82	1.2	241	2.8	14	6.4	2.3	4.0	11
		5–20	10	45	0.06	0.04	0.34	0.61	0.95	351	13	8.2	9.8	3.9	2.2	9.6
	Nodules	1–2	1	27	0.42	0.19	1.0	15	4.2	4258	30	139	103	37	68	155
		2–5	8	25	0.36	0.17	0.91	18	4.1	5860	27	227	85	55	110	144
		5–20	20	30	0.39	0.29	1.4	8.4	4.8	3357	22	125	31	53	137	76

Table 4. : Correlation coefficients for the between TE and Fe and Mn in extracts 1 and 2 and for six nodule fractions (two horizons, three nodule sizes)

***n*=6**	**Extract 1**		**Extract 2**	
	Fe	**Mn**	**Fe**	**Mn**
Mn	0.47		**0.95**	
Cr	**0.89**	0.27	**0.85**	0.69
Co	0.55	**0.90**	**0.98**	**0.98**
Ni	0.35	**0.96**	0.62	0.48
Cu	0.63	**0.95**	**0.95**	**0.85**
Zn	−0.28	0.69	**0.88**	**0.79**
Pb	0.50	0.64	−0.41	−0.39

Correlation coefficients in bold are significant at the 5% confidence level.

Table 5. : Enrichment factors in differently sized nodules (1–2 and 2–5 mm and 5 mm–2 cm) compared to the <1 mm fraction for pits 2 and 3 (P2, P3)

Pit	**Nodule size, mm**	**Si**	**Fe**	**Al**	**Ca**	**Mg**	**K**	**Mn**	**Cr**	**Co**	**Ni**	**Cu**	**Zn**	**Pb**
2	1–2	0.7	9.5	0.7	0.9	0.5	0.5	11	1.6	9.6	1.6	0.6	1.8	4.2
	2–5	0.7	9.5	0.6	0.8	0.6	0.5	15	0.9	11	2.3	0.5	1.8	3.6
	5–20	0.6	8.8	0.6	1.7	0.6	0.6	42	0.7	23	3.0	0.4	2.0	3.5
3	1–2	0.9	6.0	0.5	0.9	0.4	0.4	8.4	1.4	5.9	1.7	1.7	1.5	3.4
	2–5	0.8	7.2	0.5	0.8	0.3	0.4	12	1.2	9.6	2.5	1.6	2.4	3.2
	5–20	0.9	3.3	0.6	0.9	0.6	0.6	6.6	0.4	12	2.4	1.3	1.3	1.7

Mass balance calculations were performed using individual extracted quantities, residue and total concentrations (Table 6). These calculations show evidence of substantial losses of Ca, Zn, Cu, Ni, Co, Mn, Pb and Fe. These losses varied according to the size fraction analysed and were interpreted as colloidal losses. Filtrations were difficult after extraction 1 and filters were frequently red in colour from colloidal material. Mass balance calculations also show problems in the determination of Mn and Pb contents in extract 1 of the 5- to 20-mm nodules from pit 3.

Table 6. : Fe, Mn and TE contents in nodules and in extracts 1 and 2 and extracted residue

Pit	Nodule size	Extract	Fe %	Mn	Cr	Co	Ni mg/kg^{-1}	Cu	Zn	Pb
2	1–2 mm	Nodules	18	3595	91	113	22	35	116	138
		1	4.4	1951	20	46	5.5	6.3	15	92
		2	7.6	278	49	6.8	4.3	13	32	11
		residue	2.6	121	41	4.0	14	10	37	15
	2–5 mm	Nodules	18	4826	54	131	32	29	116	118
		1	5.6	5571	19	136	8.4	7.4	19	103
		2	8.1	468	35	8.7	3.3	12	33	13
		residue	2.5	113	43	4.3	11	10	38	14
	5 mm–2 cm	Nodules	17	13,410	43	271	42	23	128	116
		1	4.1	11,031	13	268	22	13	51	79
		2	4.5	229	23	5.9	3.9	8.6	25	5.9
		residue	1.3	82	37	3.0	11	7.3	57	14
3	1–2 mm	Nodules	15	4258	103	68	37	30	139	155
		1	3.6	3260	21	44	11	6.0	22	117
		2	6.3	250	63	6.0	8.2	13	41	15
		residue	3.7	157	45	6.6	21	17	65	25
	2–5 mm	Nodules	18	5860	85	110	55	27	227	144
		1	3.8	5447	19	76	12	6.3	22	134
		2	5.4	237	39	5.2	5.5	9.7	34	10
		residue	1.4	89	29	2.9	10	6.8	35	15
	5 mm–2 cm	Nodules	8.4	3357	31	137	53	22	125	59
		1	2.7	10,751	12	138	27	11	55	188
		2	2.6	100	19	3.0	4.5	7.6	25	5.0
		residue	0.59	46	23	1.7	8.2	4.5	22	13

Three groups of elements can be defined according to their distribution in sequentially extracted fractions. Si (>95%), Al (>70%) and K (>95%) are mainly contained in the residual phase (Table 6). This residual phase mainly consists of quartz, feldspars, micas and traces of clay minerals (Fig. 4) and is interpreted as being

(i) individual grains of quartz and feldspars contained in nodules (see below) and

(ii) cement of clay minerals.

Fifty percent of the total Ca and Mg and less than one-third of total Zn, Ni, Cu, Cr, Co, Pb, Mn and Fe were contained in the residues. In general, more than 50% of the Mn (Table 7) extracted in step 1 is associated with major proportions of Co, Pb, Ni and to a lesser extent, Mg (Table 6), while Fe is predominantly extracted in extract 2 (30% to 40%, Table 7) and is associated with Cr and Cu (Table 6). Zn is extracted in roughly equal proportions in both extracts, while Ca is essentially lost as colloids or extracted in step 1 but not in step 2.
Extracts of nodules were enriched in Mn, Fe, Co and Pb compared to the <1 mm fractions (Table 8). Fe enrichments were higher for pit 2 than for pit 3, with higher enrichments in extract 2 than in extract 1, and for small and medium size nodules than for coarse ones. Mn and Co were solely enriched in extract 1 compared to the <1 mm fractions; enrichment increasing with the nodule size. These enrichments were higher in pit 2 than in pit 3. Lead was also enriched in extract 1 only.

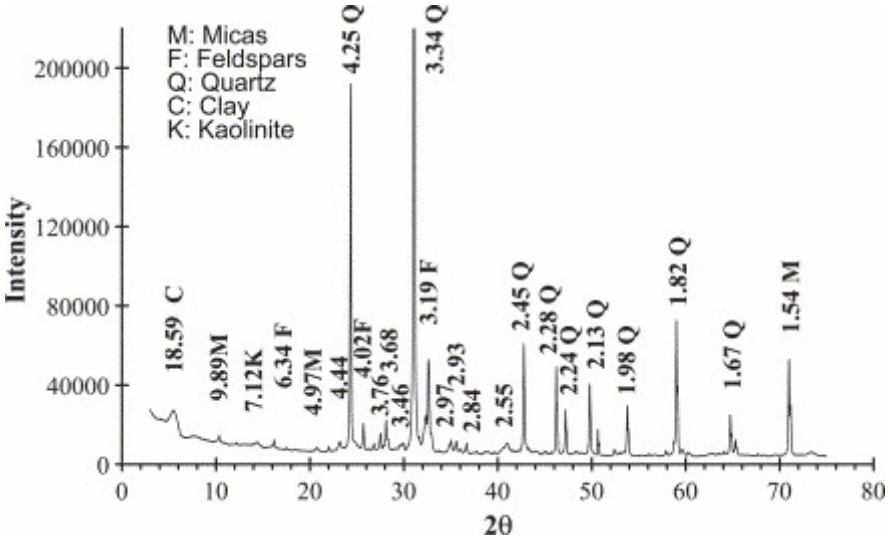

Fig. 4. XRD of the extraction residue of the 1 to 2 mm nodules from pit 2.

Table 7. : Quantities of iron and manganese present in non-crystalline (extract 1) and crystalline (extract 2) oxides and silicates (residue)

Pit	Nodule size	Fe_1/Fe_{tot}	Fe_2/Fe_{tot}	Fe_{res}/Fe_{tot}	Mn_1/Mn_{tot}	Mn_2/Mn_{tot}	Mn_{res}/Mn_{tot}
2	1–2 mm	0.2	0.4	0.1	0.5	0.08	0.03
	2–5 mm	0.3	0.4	0.1	1.1	0.10	0.02
	5 mm–2 cm	0.2	0.3	0.1	0.8	0.02	0.01
3	1–2 mm	0.2	0.4	0.2	0.7	0.06	0.04
	2–5 mm	0.2	0.4	0.1	0.9	0.04	0.02
	5 mm–2 cm	0.3	0.3	0.1		0.03	0.01

Table 8. : Enrichment factors in extracts 1 and 2 of the different nodule size fractions (1–2 and 2–5 mm and 5 mm–2 cm) compared to the <1 mm fraction of the corresponding horizon

Pit	Nodule size	Extract	Fe	Al	Mn	Cr	Co	Ni	Cu	Zn	Pb
2	1–2 mm	1	2.3	0.06	6.0	0.35	3.9	0.39	0.12	0.24	2.8
	1–2 mm	2	4.0	0.09	0.86	0.85	0.58	0.30	0.23	0.50	0.34
	2–5 mm	1	2.9	0.07	17	0.32	11	0.59	0.14	0.30	3.1
	2–5 mm	2	4.3	0.09	1.4	0.61	0.73	0.23	0.21	0.51	0.38
	5 mm–2 cm	1	2.2	0.08	34	0.23	23	1.6	0.24	0.79	2.4
	5 mm–2 cm	2	2.4	0.06	0.71	0.40	0.50	0.27	0.16	0.39	0.18
3	1–2 mm	1	1.4	0.05	6.4	0.30	3.8	0.49	0.35	0.23	2.6
	1–2 mm	2	2.5	0.07	0.49	0.87	0.52	0.37	0.74	0.43	0.32
	2–5 mm	1	1.5	0.05	11	0.26	6.6	0.56	0.37	0.24	3.0
	2–5 mm	2	2.1	0.06	0.47	0.54	0.46	0.25	0.56	0.36	0.23
	5 mm–2 cm	1	1.1	0.05	21	0.16	12	1.2	0.64	0.58	4.2
	5 mm–2 cm	2	1.0	0.04	0.20	0.26	0.26	0.20	0.44	0.26	0.11

Differential XRD patterns of nodules before and after extraction are reported in Fig. 5 and Fig. 6 for 1- to 2-mm and 5- to 20-mm nodules from pit 2, respectively. Fig. 5 shows broad peaks that were attributed to ferrihydrite and goethite. These peaks are of smaller intensity for the 5- to 20-mm nodules. No differences were observed between nodules of the two pits. Mn oxides could not be identified.

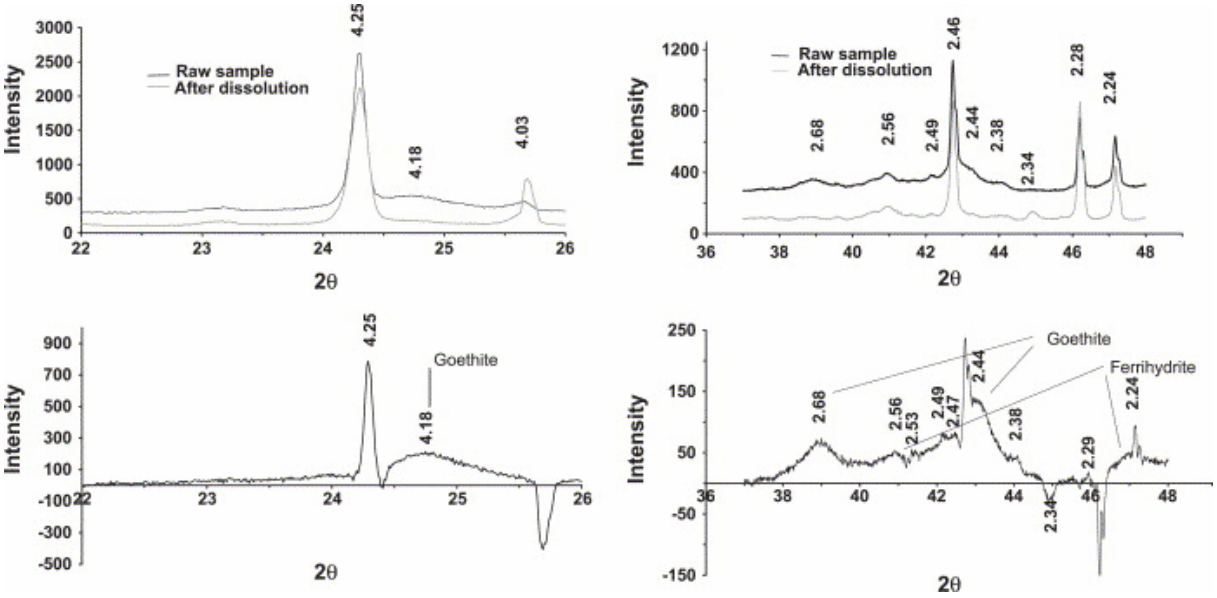

Fig. 5. Difference of the X-ray diffractograms before and after sequential extractions. Example of 1 to 2 mm nodules from pit 2.

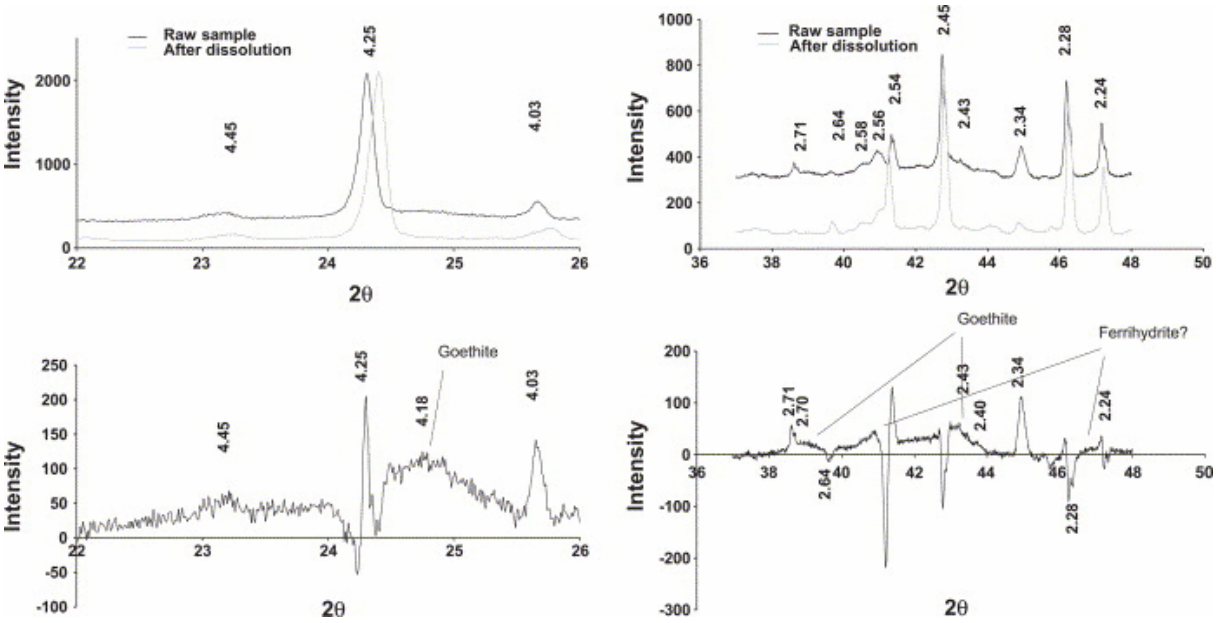

Fig. 6. Difference of the X-ray diffractograms before and after sequential extractions. Example of 5 to 20 mm nodules from pit 2.

3.3. Characterisation of the nodules: microscopic approaches

Most of the nodules observed are irregular in shape, either black or pale reddish in colour and consist of soil grains cemented by oxides. The grains are mainly quartz but also include feldspars, micas and accessory minerals. The

oxide matrix is mainly composed of Fe, Al and Si, with minor amounts of Ti and Mn. This composition varies according to the nodule type and also within a given nodule. Some nodules show concentric bands of different composition as shown in Fig. 2A and B and partially in Fig. 2E. However, most of them do not exhibit a clear inner structure (Fig. 2C and D). The maps presented in Fig. 2 clearly show that Fe, Si, Al, Mn and Ti are unevenly distributed within the nodules. Iron-rich parts are generally depleted in other elements, while Ti- or Mn-rich parts are often richer in Si and Al than the remainder of the nodule. Uneven spatial distribution of the elements is also encountered in unbanded nodules (Fig. 2C, D and E).

A PCA was performed on the 51 punctual chemical analyses obtained on the nodule matrix. As the correlation circle of the PCA (Fig. 7) shows, the first two factors explain 48% of the variability, 35% being explained by the first factor. This factor defines two main poles comprising Fe and Al, Si, Mg, K respectively. The second factor explains about 13% of the variability and is mainly defined by a pole comprising Mn, Pb . Cement that is rich in both Si and Al has a Si/Al ratio generally equal to 1. XRD shows that the nodules contain a small amount of kaolinite. PCA differentiates three types of cements: cements rich in Fe, cements rich in Mn and Pb and cements composed at least in part of kaolinite. These results were not in complete agreement with those obtained by chemical analysis as Co was not associated to the Mn pole. However, the measured content of Co was often close to or less than the detection limit of the electron microprobe.

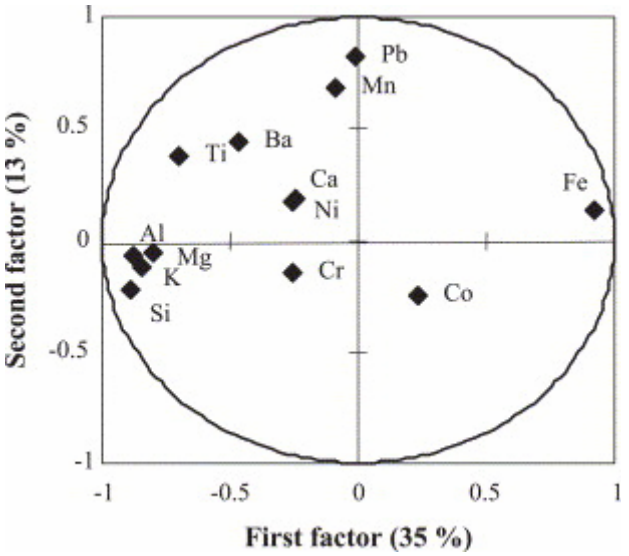

Fig. 7. Principal component analysis of chemical composition obtained by microanalysis associated with back-scattered electron microscope.

4. Discussion

4.1. Location of TE in the nodules

Results obtained by sequential extractions and associated XRD on the different nodule size fractions and those obtained by electron microprobe allow inference of the TE distribution in nodules. Nodules were mainly composed of three to four types of cements (iron-rich, Si- and Al-rich, Mn-rich and Ti-rich) surrounding grains of quartz, feldspars, micas and accessory minerals.

The iron-rich cements consist of poorly crystalline goethite and possibly some ferrihydrite, as also observed by Liu et al. (2002) in other nodules. According to Hall et al. (1996), ferrihydrite dissolves in extract 1. It is associated with Cr as demonstrated by the correlation coefficients (Table 4). Goethite was dissolved in extract 2 (Hall et al., 1996) and contained Mn and most of the TE extracted, except for Ni and Pb (Table 4).

Fine-grained Si- and Al-rich cements were also observed (Fig. 2 and Fig. 7). They are probably kaolinite (XRD, not shown) but could also partially exist as amorphous phases as shown by the small percentage of these elements extracted. Such amorphous Si- and Al-rich products were also observed by Bulmer and Lavkulich (1994). These cements contain variable amounts of Ti and Mn as seen by electron microprobe analyses (Fig. 2).

Mn-rich cements were not present in all the nodules as seen in Fig. 2 and were mainly linked to the dark zones of the nodules. Mn oxides could not be identified by XRD. According to Taylor (1968), birnesite and lithiophorite are the most frequent forms in nodules. The correlation statistics suggest that the Mn oxides contain Co, Ni, Cu (Table 4) and probably Pb (Table 8 and Fig. 7). Co is classically found to be associated with Mn oxides (Taylor, 1968, Yaalon et al., 1974, Childs and Leslie, 1977, Means et al., 1978, McKenzie, 1989, Latrille et al., 2001, Liu et al., 2002 and Palumbo et al., 2001) as are Ni and Cu (Latrille et al., 2001, Liu et al., 2002 and Palumbo et al., 2001). Contradictory results are reported for Pb. It was shown by Latrille et al. (2001) to be associated with Fe, while McKenzie (1989) and Liu et al. (2002) mentioned an association between Pb and Mn oxides.

Compositions of nodules were compared to the <1 mm fractions in order to estimate the role of these nodules as a sink for the different elements. Co was preferentially associated with the Mn oxides, with a slight Pb enrichment also observed (Table 8). Iron was also accumulated in nodules although to a lesser extent than Mn (Table 7). The principal form of iron in the nodules was goethite (demonstrated by the larger amount of Fe extract by step 2; Table 7) and some ferrihydrite was also present. However, Fe enrichment factors for these phases (Table 8) are half those recorded for this element in the whole nodule (Table 5). The extraction procedure may have been incomplete for

this element and resistant crystalline iron may remain in the residue, as shown by the 10% to 20% of Fe present in this component (Table 7). This was, however, not evident from X-ray diffraction.

Nodules from both profiles were slightly enriched in Ni and Zn, and also in Cu in profile 3 only (Table 5). This is in agreement with results recorded by Childs and Leslie (1977). Neither the Fe nor the Mn oxides were enriched in these TE. These oxides may not have been completely extracted as already discussed for Fe. Cr and other major elements analysed were depleted compared to the <1 mm fractions. Such a depletion was also recorded by Childs and Leslie (1977) for Si, Al, K and Ca. Bulmer and Lavkulich (1994) showed that Cr released from primary minerals by weathering was mainly incorporated in clays and less so in iron oxides.

The nodule composition varied according to their size and location on the slope. The content of Mn oxides in nodules increased with their size and was higher in profile 2 than 3. Nodules in profile 2 were also richer in iron oxides, with small and medium size nodules containing the largest proportion. Almost all the nodules analysed by electron microprobe were small nodules, explaining the small amount of Mn cements encountered.

The spatial segregation observed between Mn and Fe within the nodules is also encountered among the different nodule sizes. In addition, nodules appeared to be a sink for Fe, Mn, Co, Pb, Ni, Zn and sometimes, Cu.

4.2. TE distribution along the slope in relation to the water regime

Surface allochthonous horizons are quite similar in depth and along the toposequence. They were mainly differentiated by their thickness due to erosion (Salvador-Blanes, 2002). They could be roughly considered as the initial composition of the allochthonous horizons before the Planosol differentiation. For that reason, they were used as a reference in the enrichment factor calculation. The nodule-rich horizons were enriched in Mn, Co, Fe and in some cases, Pb, Ni, and Cu also. All of them were depleted in Cr and Zn and in most major elements. This might be interpreted as precipitation of Fe and Mn oxides in this coarse horizon, inducing soil grain cementing and nodule formation. These nodules are predominantly enriched in Fe, Mn and Co and are slightly enriched in Pb, Ni and Zn compared to the <1 mm fractions of the same horizons. These Pb, Ni and Zn enrichments are not sufficient to enrich this horizon in these elements.

In addition, the enrichment in Fe, Mn and Co varies along the toposequence and with depth. Maximum enrichments were recorded in pit 2 for Fe and in pit 3 for Mn. This result is in apparent contradiction with previous data, which indicated a maximal enrichment in Mn and Co in pit 2 (Tables 5 and 8). Nodules were analysed from the E_3 horizon only. This horizon was richer in Mn, Fe and Co than the overlying E_2 in pit 2, but was poorer in those elements in

pit 3 (Table 1). The E_2 in pit 2 was depleted in Fe, Mn and Co. This distribution of Fe, Co and Mn along the slope was related to the water regime and waterlogging of this soil. These soils are waterlogged during winter and spring, the duration of which increases along the slope. In pit 1, the waterlogging period is short and only a small amount of Fe and Mn are mobilised and precipitated as nodules. In pit 2, this period is somewhat longer inducing release of Fe and Mn from the E_2 horizon, which precipitate in the underlying E_3 horizon or migrate downslope. Downslope migration is probably limited, as shown by the almost constant stocks recorded for Mn and Fe along the toposequence. In pit 3, the waterlogging period is at a maximum. The majority of Fe and Mn are accumulated in the E_2 horizon. The E_3 horizon undergoes a long reducing period that prevents large Mn accumulation.

5. Conclusion

In this work, TE distribution in Planosols along a toposequence was analysed. Three pits were opened and described. Main horizons were sampled and chemically analysed. A nodule-rich horizon was present in all three pits. It differentiates, from the middle part of the slope downwards, into 2 horizons, named E_2 and E_3, respectively. The latter were studied in greater detail in order to locate the TE and to characterise the nature of the oxides forming the nodule cements.

The nodule-rich horizon is a sink for Fe, Mn, Co and Pb and also for Ni and Cu in places. The scavenging efficiency of this horizon varies along the slope and according to the element considered. The scavenging effect is only evident for Ni in pit 1. For Fe and Cu, it is maximal in pit 2 where the nodule-rich horizon is the thickest. For Pb and Mn, maximal scavenging effect is recorded for both pits 2 and 3, i.e., in the lowest part of the slope. Cr is not accumulated at all.

This element behaviour is partially explained by the TE speciation in the nodule-rich horizon. Cr is not preferentially contained in nodules; its fate along the slope is governed by erosion/deposition processes of clay minerals. Half of the Cu and Zn are contained within nodules. The Cu is in association with crystalline iron oxide, probably goethite, which has accumulated in pit 2. Zn accumulates in both goethite and non-crystalline iron oxides, probably ferrihydrite. Lastly, Mn oxides preferentially scavenge Co, Pb and Ni. The mineralogical nature of these oxides could not be determined.

Working at different scales allows

(i) determination of the different phases containing TE,

(ii) determination of their distribution within the toposequence, and

(iii) for understanding of the soil formation and its subsequent probable evolution.

Aknowledgment

The authors would particularly like to thank O. Josière and C. Le Lay for technical support.

References

Alloway, 1990 B.J. Alloway In: J. Blakie, Editors, *Heavy Metals in Soils*, Wiley & Sons, Glasgow (1990) 339 pp..

Baize, 1989 Baize, D., 1989. Planosols in the "Champagne Humide" region, France. A multi-approach study. Pédologie, XXXIX-2, Ghent, pp. 119–151.

Bulmer and Lavkulich, 1994 C.E. Bulmer and L.M. Lavkulich, Pedogenic and geochemical processes of ultramafic soils along a climatic gradient in southwestern British Columbia, *Canadian Journal of Soil Science* **74** (1994), pp. 165–177.

Cambier and Charlatchaka, 1999 P. Cambier and R. Charlatchaka, Influence of reducing conditions on the mobility of divalent trace metals in soils In: H.M. Selim, Editors, *Fate and Transport of Heavy Metals in the Vadose Zone*, Lewis Publishers, Boca Raton (1999), pp. 159–175.

Chao and Theobald, 1976 T.T. Chao and J. Theobald, The significance of secondary iron and manganese oxides in geochemical exploration, *Economic Geology* **71** (1976), pp. 1560–1569.

Childs and Leslie, 1977 C.W. Childs and D.M. Leslie, Interelement relationships in iron–manganese concretions from a catenary sequence of yellow-grey earth soils in loess, *Soil Science* **123** (1977) (6), pp. 369–376.

Dario and Ledin, 1997 M. Dario and A. Ledin, Sorption of Cd to colloidal ferric hydroxides—impact of pH and organics acids, *Chemical Speciation and Bioavailability* **9** (1997) (1), pp. 3–14.

Dawson et al., 1985 B.S.W. Dawson, J.E. Fergusson, A.S. Campbell and E.J.B. Cutler, Distribution of elements in some Fe–Mn nodules and an iron-pan in some gley soils of New Zealand, *Geoderma* **35** (1985), pp. 127–143.

Hall et al., 1996 G.E.M. Hall, J.E. Vaive, R. Beer and M. Hoashi, Selective leaches revisited, with emphasis on the amorphous Fe oxyhydroxide phase extraction, *Journal of Geochemical Exploration* **56** (1996), pp. 59–78.

Jenne, 1968 E.A. Jenne, Controls on Mn, Fe, Co, Ni, Cu and Zn concentrations in soils and waters: the significant role of hydrous Mn and Fe oxides In: R.F. Gould, Editors, *Trace Inorganics in Water*, Adv. Chem. American Chemical Society, Washington (1968), pp. 337–387.

Latrille et al., 2001 C. Latrille, F. Elsass, F. van Oort and L. Denaix, Physical speciation of trace metals in Fe-Mn concretions from a rendzic lithosol developed on Sinemurian limestones (France), *Geoderma* **100** (2001) (1/2), pp. 127–146.

Liu et al., 2002 F. Liu, C. Colombo, P. Adamo, J.Z. He and A. Violante, Trace elements in manganese–iron nodules from a Chinese Alfisol, *Soil Science Society of America Journal* **66** (2002), pp. 661–670.

Loganathan et al., 1977 P. Loganathan, R.G. Burau and D.W. Fuerstenau, Influence of pH on the sorption of Co^{2+}, Zn^{2+} and Ca^{2+} by a hydrous manganese oxide, *Soil Science Society of America Journal* **41** (1977), pp. 57–62.

McBride, 1994 M.B. McBride, Environmental Chemistry of Soils, Oxford University Press, Oxford (1994) 406 pp..

McKenzie, 1975 R.M. McKenzie, An electron microprobe study of the relationships between heavy metals and manganese and iron in soils and ocean floor nodules, *Australian Journal of Soil Research* **13** (1975), pp. 177–188.

McKenzie, 1989 R.M. McKenzie, Manganese oxides and hydroxides, *Minerals in Soil Environments*, *SSSA Book Series*, Soil Science Soc. of Am, Madison (1989), pp. 439–465.

Means et al., 1978 J.L. Means, D.A. Crarar and M.P. Borcsik, Adsorption of Co and selected actinides by Mn and Fe oxides in soils and sediments, *Geochimica et Cosmochimica Acta* **42** (1978), pp. 1763–1773.

Oades, 1963 J.M. Oades, The nature and distribution of iron compounds in soils, *Soils Fertilizers* **26** (1963), pp. 69–80.

Palumbo et al., 2001 B. Palumbo, A. Bellanca, R. Neri and M.J. Roe, Trace metal partitioning in Fe–Mn nodules from Sicilian soils, Italy, *Chemical Geology* **173** (2001), pp. 257–269.

Salvador-Blanes, 2002 Salvador-Blanes, S., 2002. Déterminisme de la distribution spatiale des éléments majeurs et traces dans les sols en contexte métamorphique. PhD thesis, University of Tours, Tours.

Schulze, 1981 D.G. Schulze, Identification of soil iron oxide minerals by differential X-ray diffraction, *Soil Science Society Of America Journal* **45** (1981), pp. 437–440.

Schwertmann et al., 1989 U. Schwertmann, U. Gasser and H. Sticher, Chromium-for-iron substitution in synthetic goethites, *Geochimica et Cosmochimica Acta* **53** (1989), pp. 1293–1297.

Singh and Gilkes, 1992 B. Singh and R.J. Gilkes, Properties and distribution of iron oxides and their association with minor elements in the soils of southern-Australia, *Journal of Soil Science* **43** (1992), pp. 77–98.

Taylor, 1968 R.M. Taylor, The association of manganese and cobalt—further observations, *Journal of Soil Science* **19** (1968) (1), pp. 77–80.

Trolard et al., 1995 F. Trolard, G. Bourrié, E. Jeanroy, A. Herbillon and H. Martin, Trace metals in natural iron oxides from laterites: a study using selective kinetic extraction, *Geochimica et Cosmochimica Acta* **59** (1995) (7), pp. 1285–1297.

Yaalon et al., 1974 D.H. Yaalon, I. Brenner and H. Koyumdjinsky, Weathering and mobility sequence of minor elements on a basaltic pedomorphic surface, Galilee, Israel, *Geoderma* **12** (1974), pp. 233–244.